Adsorbed CO on Group 10 Metal Fragments: A DFT Study†

Sergio Giuffrida, Giampaolo Barone, and Dario Duca*

Dipartimento di Chimica Inorganica e Analitica "S. Cannizzaro" dell'Università di Palermo, viale delle Scienze Ed. 17, I-90128 Palermo (Sicily), Italy

Received December 26, 2008

DFT calculations on the helicopter and cartwheel rotations of one CO molecule adsorbed at the bridge site on metal-surface fragments, characterized by two (M_8) or three (M_{14}) metal-atom layers (M = Ni, Pd, Pt) were performed by the B3LYP[LANL2DZ+6-31 g(d,p)] method, to rationalize the adsorption energetics and the steric hindrance characteristics of surface CO molecules. Potential Energy Surfaces were obtained, either fixing the C-O bond-length or allowing it to change. The behavior of the three metals, as obtained from the study of the configurational space characterizing the CO adsorption on the fragments was explained on the basis of the interaction energies involved in the different CO/M systems. The results, obtained by using the M_{14} fragments and varying both the C-O and the CO/M distances, point out that the CO adsorption on the Ni fragment is stabilized by surface-configurations in which the O atom is pointing toward a metal center. At variance, C-O bond elongation and stabilization occur on Pd when the O atom is situated between two palladium atoms. The CO adsorption on Pt displays similar characteristics to those observed on the Pd systems, but with the fundamental difference caused by the destabilization of the Pt-O interactions when the O atom is situated exactly between two Pt atoms. The calculations allowed us to estimate the IR spectroscopy frequency and band-broadening of the adsorbed CO stretching by a statistic analysis on a large set of energy ÷ bond-length computed data. Good agreement with the experimental results was obtained for all the metals, in particular concerning the frequencies. Reliable band-broadenings were also obtained for the CO/Ni and CO/Pt systems, while the lower band-broadening value for the CO/Pd system was related to the small extent of the configurational sampling space.

INTRODUCTION

The need to get high activity and selectivity performances in heterogeneous catalytic reactions requires a thoroughly understanding of the elementary phenomena involved in the surface processes. Molecular-level information is useful in designing the catalytic site geometry and the substrate feed composition as well as the optimization of elementary steps, characterizing the apparent macroscopic reactions.[1] With respect to the latter, the role of the steric hindrance in studying surface and catalytic processes is at present widely discussed in the literature.[2−4]

In order to study the adsorption of CO on metal surfaces, several quantum chemical (QC) models have up to now been proposed and utilized.[5−7] In most cases these models account just for single conformational modes of CO adsorption, without allowing for molecular bending and/or rotation on the surface, thus implicitly assuming the process as realized at 0 K and being the stablest surface-configuration the only occupied state. Therefore, to consider the molecular steric hindrance of adsorbed species, more realistic surface models have to be taken into account. In particular, the steric-hindrance of CO adsorbed on metal surfaces can be mimicked, taking into consideration the "helicopter rotation" (or horizontal rotation)[3] and the "cartwheel rotation" (or azimuthal bending),[8] schematically represented in Figure 1

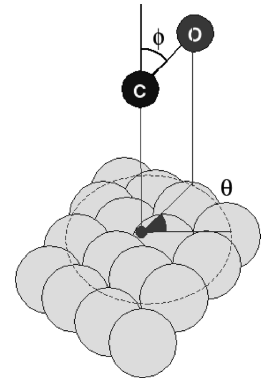

Figure 1. CO rotation angles involved in the helicopter (angle θ) and cartwheel (angle ϕ) motions -- the carbon monoxide molecule and the metal-surface fragment are not in scale.

by the angles θ and ϕ, respectively. These molecular motions occur very close to the surface plane and affect the energetic and the reactivity properties of the adsorbed species,[3] locally modifying the steric hindrance. This confirms that a larger distribution of possible surface-configurations has to be considered to adequately manage both spectroscopical and chemical properties of the surface CO arrangements.

The investigation of the CO adsorption on clusters and crystallite surfaces of the Group 10 metals has an extreme relevance because of the importance of these metals in technical applications, especially in catalysis.[3,9] In fact, CO adsorption is a crucial step for several reactions of technical, industrial, and environmental interest,[10] which involve either oxidation, e.g. automotive processes,[11] or hydrogenation, e.g.

* Corresponding author e-mail: dduca@cccp.unipa.it.

† Dedicated to the memory of Adolfo Parmaliana, colleague and friend, deceased October 2, 2008.

10.1021/ci800469m CCC: $40.75
Published on Web 04/30/2009

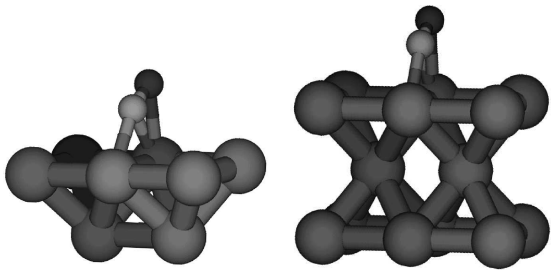

Figure 2. Structures of the two considered systems at $\theta = 0°$: CO/M_8 on the *left* and CO/M_{14} on the *right* (M = Ni, Pd, Pt), the ϕ value is 0° for CO placed perpendicularly to the metal plane -- C in light-gray, O in dark-gray, metal atom in midgray. The crystallite fragments differ just for the presence of the third metal-atom layer.

Fischer−Tropsch processes.[12] Carbon monoxide is further used as a local probe molecule to characterize metal fragments and clusters because of the relative simplicity in the interpretation of its spectral properties. Indeed, the CO IR spectrum is particularly sensitive to the C-O bond order and binding type, and the C-O stretching band falls in a "clean" region of the vibrational spectrum. For such reasons, the CO stretching band has become one of the most known and studied IR bands in coordination and cluster chemistry.[13]

In this work we report on QC calculations of a set of CO/metal-fragment (CO/M_n) systems, with the aim to model and rationalize different aspects of the CO bridge adsorption process on the surfaces of the Group 10 metals, accounting also for the steric hindrance effects. For each metal, two fragment types have been taken into consideration: one M_8 (two-layers) system and one M_{14} (three-layers) system. The study of the larger fragment was performed even allowing the change of the C-O bond-length. As a consequence, detailed maps, namely potential energy surface (*PES*) and elongation surface plot (*ESP*), respectively, of the energy (E) and of the carbon monoxide bond-length (d_{CO}) values have been obtained, depending on the considered helicopter and cartwheel rotation angles (θ and ϕ, as stated above). For these systems, three different carbon monoxide metal-atom distances (d_{M_2C}) were considered for each metal, to get an evaluation also of the effect of the CO/M distance. The consequent analysis showed the fundamental role of both d_{CO} and d_{M_2C} elongations to define the CO/M_n physical models. Each couple of maps -- $PES(\theta,\phi) + ESP(\theta,\phi)$ -- for a given metal system provided a set of $E \div d_{CO}$ data couples, which allowed us to carry out a statistical evaluation of Morse potential parameters -- see the Supporting Information -- useful in reconstructing the CO band stretching frequency and broadening, taking into consideration a large population among the possible surface-configuration states.

Model and Computational Details. Both the M_8 (two-layers) and the M_{14} (three-layers) fragments were cut from an ideal metal structure to obtain {100} faces.[14] The corresponding experimental metal−metal (M-M) bond-lengths (249, 275, and 277 pm for Ni, Pd, and Pt) and angles were not allowed to change along the calculations. The CO molecule has been considered just in the bridge adsorption configurations, mainly because experimental findings have shown that hollow as well as atop adsorption should be less probable in occurring on populated surfaces,[15,16] i.e. those of practical interest. Examples of the considered structural geometries of the CO/M_n fragments are shown in Figure 2.

Table 1. Distance Parameters of CO Adsorbed on Group 10 Metal Surfaces

M_8 | M_{14} fragments[a]	d_{CO}/pm	d_{M_2C}/pm[b]	d_{MC}/pm[c]
Ni systems	118 | 118	133 | 135	182 | 183
Pd systems	117 | 117	138 | 151	194 | 204
Pt systems	118 | 118	140 | 147	197 | 203

[a] Partially optimized distance values characterizing the carbon monoxide molecule adsorbed on M_8 and M_{14} fragments (M_8|M_{14}). [b] d_{M_2C} is the distance between the center of mass, i.e. the bridge contact point (*bcp*), of the two metal atoms, individuating the central M-M bond along the smallest side of the metallic fragment, and the bridge interacting C atom of the CO/M_n systems. [c] d_{MC}, calculated averaging on a couple of the M-C distance values obtained on the central M sites - of the upper plane in the fragment - is reported in order to have a direct comparison with the corresponding geometrical parameters reported in the literature.[17,18]

All the calculations were performed, as already done for very similar model systems, in the singlet state[17,18] by the Gaussian03 suite of programs,[19] employing the hybrid B3LYP method[20] with the extended split-valence double-ζ 6-31G(d,p) basis set for the carbon and oxygen atoms and the LANL2DZ pseudopotential basis set,[21] partly accounting for scalar relativistic effects,[22] for the metal atoms. Nonhybrid functionals, in the frame of either the Local Density Approximation (LDA) or the Generalized Gradient Approximation (GGA),[23] and Periodic Boundary Conditions (PBC)[24] have not been taken into consideration here, since it has been reported that for this kind of systems they experience problems, at variance with the B3LYP method,[6] in determining the right adsorption sites from the calculated adsorption energies.[7] For each couple of θ and ϕ angles, a single point calculation, at fixed d_{CO}, or a set of single point calculations, at variable d_{CO}, were performed and employed for constructing the $PES(\theta,\phi)$ plots.

Partial optimizations of the adsorbed CO geometry were also carried out on both the CO/M_8 and CO/M_{14} systems, taking fixed the geometry of the metal fragments. The carbon monoxide molecule, irrespective of the involved metal and fragment sizes, resulted optimized at $\phi = 0°$. The remaining optimized parameters, namely the C-O distance, d_{CO}, and the CO/M distance, d_{M_2C}, are reported in Table 1. This shows that although the d_{CO} values are constant in the M_8 and M_{14} systems, the d_{M_2C} values undergo changes as large as 9% in the same fragments. However, both the d_{M_2C} and the d_{MC} as well as the d_{CO} distance values for the different M_8 and M_{14} systems show a general good agreement with similar calculated parameter values already reported for analogous fragments and clusters, exceeding, only in one case, percentage variations larger than 2.5%.[17,18] Moreover, the calculated adsorption energy values, 119, 143, and 72 kJ mol^{-1}, obtained for the Ni_{14}, Pd_{14}, and Pt_{14} fragments, considering the BSSE correction,[25] are well in the range of the corresponding experimental values reported for the Ni[16] and Pd[26] {100} faces. In the case of Pt, the energy obtained is in the lowest limit of the experimental range,[27] but it is in line with calculated values found in the literature for the interaction energy between CO and Pt clusters.[18] Straightforwardly, the considerations above confirm the reliability of the B3LYP method employed here.

The d_{M_2C} value was not allowed to change along the $PES(\theta,\phi)$ calculations. However, we monitored the CO/M_n

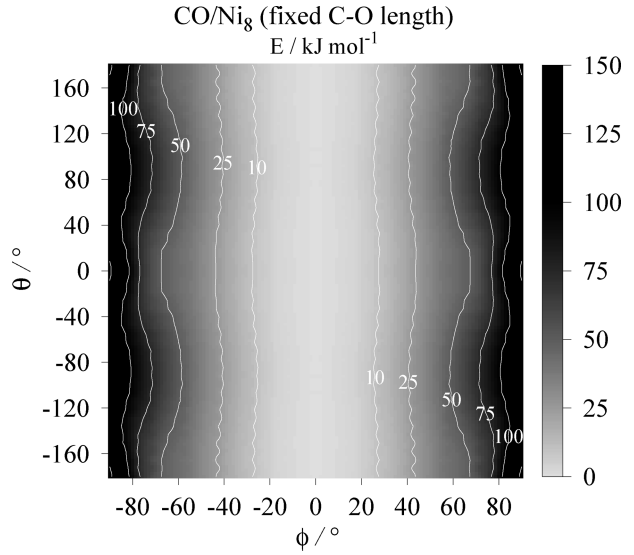

Figure 3. *PES*(θ,ϕ) of the CO rotation (θ) and bending (ϕ) on the Ni_8 fragment surface: d_{CO} is fixed at 116/pm, d_{M_2C} at 165/pm. The zero of energy ($E_0 = -1467.5416$ au) corresponds to the stablest surface-configuration.

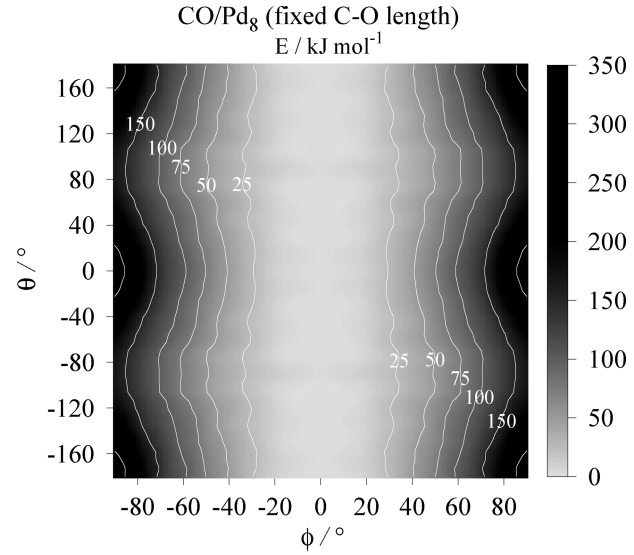

Figure 4. *PES*(θ,ϕ) of the CO rotation (θ) and bending (ϕ) on the Pd_8 fragment surface: d_{CO} is fixed at 116/pm, d_{M_2C} at 165/pm. The zero of energy ($E_0 = -1127.2514$ au) corresponds to the stablest surface-configuration.

systems at different d_{M_2C} values in order to test the effects of the θ and ϕ rotation angles on the CO/M equilibrium distances. Consequently, to study the M_{14} fragments, the d_{M_2C} values were fixed at their equilibrium distances -- see Table 1 -- as well as at 165 and 195 pm. The latter distances were chosen to allow weaker repulsive interactions between the CO oxygen atom and the metal surface at higher bending angles, thus trying to simulate the helicopter and cartwheel rotations at longer adsorption distances. In fact, increasing the adsorption distances, for large $|\phi|$ angles, the corresponding $E(\theta,\phi)$ values become smaller than the energies of the corresponding equilibrium configurations.

To summarize, adsorption of CO on M_8 and M_{14} systems have been studied by the B3LYP *PES*(θ,ϕ) analyses at fixed d_{M_2C} and d_{CO} values to elucidate the effect of the size of the involved fragment. Whereas, *PES*(θ,ϕ) plots varying both the distance parameters above have been considered for the larger systems to analyze the influence of the molecular readjustments on the adsorption energy, occurring along the surface rotations. Moreover, as explained in the Supporting Information, the study of the larger fragment at variable C-O bond-lengths allowed us to obtain a couple of parallel *PES* and *ESP* maps that for a given metal system provided a set of $E \div d_{CO}$ couples, enabling a new IR computational analysis able to fix frequency and band-broadening values of carbon monoxide adsorbed on Group 10 metal surfaces.

RESULTS AND DISCUSSION

The *PES*(θ,ϕ) plots[28] obtained by employing the M_8 fragments at a fixed CO bond-length are shown in Figure 3 − 5, whereas those of the M_{14} systems are reported in Figure 6 − 8, for the fixed d_{CO} analysis and in Figure 9 − 11, for the variable d_{CO} analysis. Finally, the IR band frequency and broadening reconstruction are reported and discussed in the last section.

By the inspection of the whole set of figures above, the energy involved in the azimuthal bending would seem restricted within 0° ÷ ±10° at 300 K on monoadsorbed surfaces, irrespective of the considered metallic systems.

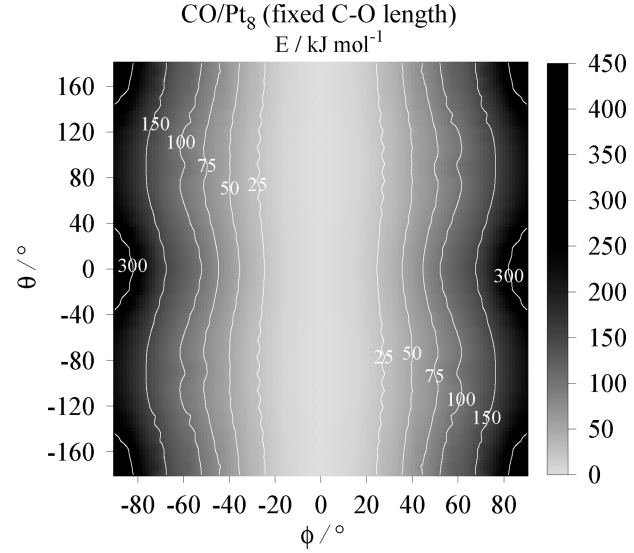

Figure 5. *PES*(θ,ϕ) of the CO rotation (θ) and bending (ϕ) on the Pt_8 fragment surface: d_{CO} is fixed at 116/pm, d_{M_2C} at 165/pm. The zero of energy ($E_0 = -1066.4842$ au) corresponds to the stablest surface-configuration.

However, for more realistic models, at the same average temperature above, assembled by extended and variously populated Group 10 metal {100} planes that undergo CO hitting and diffusion as well as adsorption and desorption at atmospheric pressure, it was recently demonstrated[3] that in the near surroundings of their adsorption sites the CO molecules can experience much higher temperature. Local hot spots (and in general temperature gradients) could indeed be produced by mutual energies transfer arising among metal particles and adsorbed molecules, through the occurrence of the surface events.[3,29] The so produced surface hot spots should be able to transfer energy to adsorbed carbon monoxide molecules hence to bend them to larger angles[3] (even up to ±90°).

Adsorption of CO on M_8 Fragments. In order to analyze average conditions, models having $d_{M_2C} = 165$ pm were initially considered for the fixed d_{CO} M_8 and M_{14} systems.

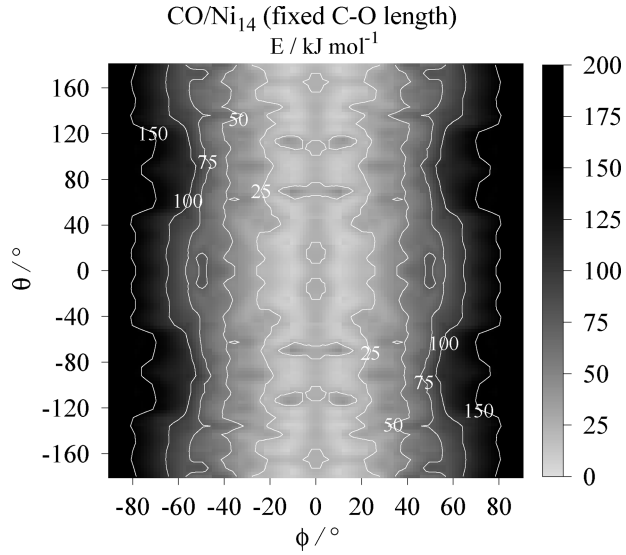

Figure 6. *PES*(θ,ϕ) of the CO rotation (θ) and bending (ϕ) on the Ni_{14} fragment surface: d_{CO} is fixed at 116/pm, d_{M_2C} at 165/pm. The zero of energy ($E_0 = -2483.3266$ au) corresponds to the stablest surface-configuration.

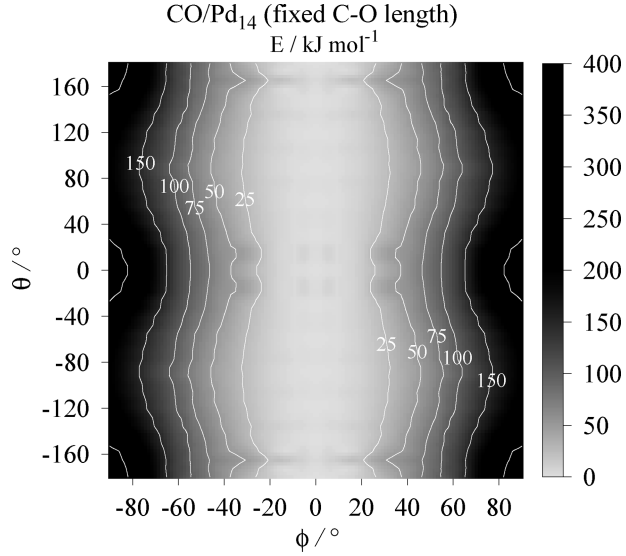

Figure 7. *PES*(θ,ϕ) of the CO rotation (θ) and bending (ϕ) on the Pd_{14} fragment surface: d_{CO} is fixed at 116/pm, d_{M_2C} at 165/pm. The zero of energy ($E_0 = -1887.7922$ au) corresponds to the stablest surface-configuration.

In the M_8 fragments (Figure 3−5), it is evident that the helicopter rotation influences only slightly the energy at a small azimuthal bending, and only at high $|\phi|$ angles it is possible to observe an effect of the θ angles. Indeed, the energy values at high $|\phi|$ are different for the three metals, with an increasing trend that rises from Ni to Pt. So, the maximum interaction energy value obtained for the Ni_8 system is ca. 150 kJ mol^{-1}, far less than the one for the Pd_8 and Pt_8 systems, which are ca. 350 and 450 kJ mol^{-1}, respectively.

Moreover, by analyzing the energy profiles at large $|\phi|$ angles, it is possible to notice other differences in the properties of the three metals, having Pd and Pt more similar behavior. On both these metals, very bent molecules are not probable around $\theta = 0°$ or $\pm 180°$ because of the high energy barriers involved. For these systems, the lowest energy values are found at $\theta = \pm 90°$. This indicates that, when CO is

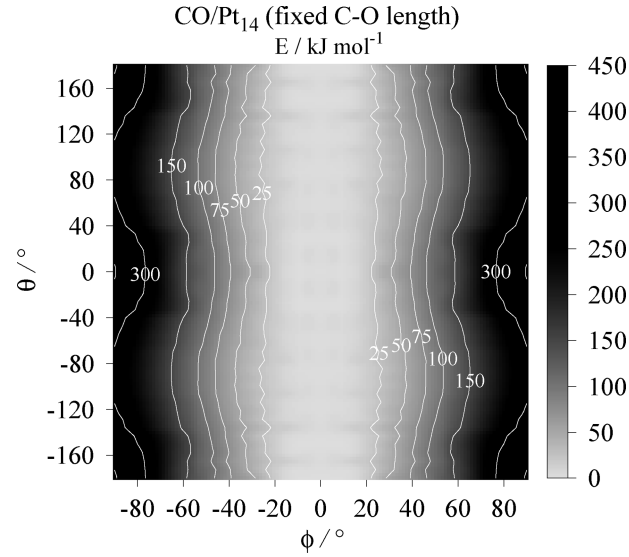

Figure 8. *PES*(θ,ϕ) of the CO rotation (θ) and bending (ϕ) on the Pt_{14} fragment surface: d_{CO} is fixed at 116/pm, d_{M_2C} at 165/pm. The zero of energy ($E_0 = -1781.4559$ au) corresponds to the stablest surface-configuration.

bridge-bound on Pd_8 or Pt_8 fragments, the cartwheel bending draws preferentially the O atom to interact with a couple of second neighboring metal atoms.[30]

The bending effects of CO on the Ni surface is significantly different, since at intermediates $|\phi|$ angles ($50° < |\phi| < 75°$) the preferential bending positions are at $\theta = 0°$ and $\pm 180°$, corresponding to a single interaction of the oxygen atom with first neighboring metal atoms. At higher bending angles, $|\phi| > 75°$, these configurations become unstable, in favor of those at $\theta = \pm 45°$ or $\pm 135°$, which correspond always to a single interaction of the oxygen atom, but shifted from the first to the second neighboring metal atoms. The configuration stability shift can be explained considering that the C-O bond-length is fixed in these systems and the Ni-O distance with the first neighbor nickel atoms becomes too short at higher $|\phi|$.

Adsorption of CO on M_{14} Fragments at Fixed C-O Distance. The *PES*s obtained by the M_{14} fragments are shown in Figures 6−8. On the whole, at a given θ and ϕ angles the energies in the M_{14} fragments are larger than those observed in the M_8 ones. This leads to differences in the evaluation of the accessible bending angles, hence in the evaluation of the characteristics surface steric hindrance of the adsorbed molecule. Besides, the isoenergetic lines are more fractured in the M_{14} systems, in particular at lower $|\phi|$ angles, showing irregularities to be probably referred to the model approximations, namely to the fixed d_{CO} and d_{M_2C} values. Interestingly, an inconsistency emerges in Figure 6: at $\phi = 0°$ it is actually observed a slightly no constant behavior, changing with the θ values. This unphysical trend, also observed in Figures 9 and 11, has no influence on the whole analysis and is due to the unconstrained fits carried out to get the *PES* and *ESP* plots. In fact, we did not impose any restriction to the protocol used to obtain the latter, forcing to "the expected behaviour" the offset points of the constant $\phi = 0°$ isohypse lines.

It is evident from the comparison of the two system sets that the *PES*s of the M_8 systems are smoother in the case of the Ni fragments, while the *PES*s of the Pd_{14} and Pt_{14}

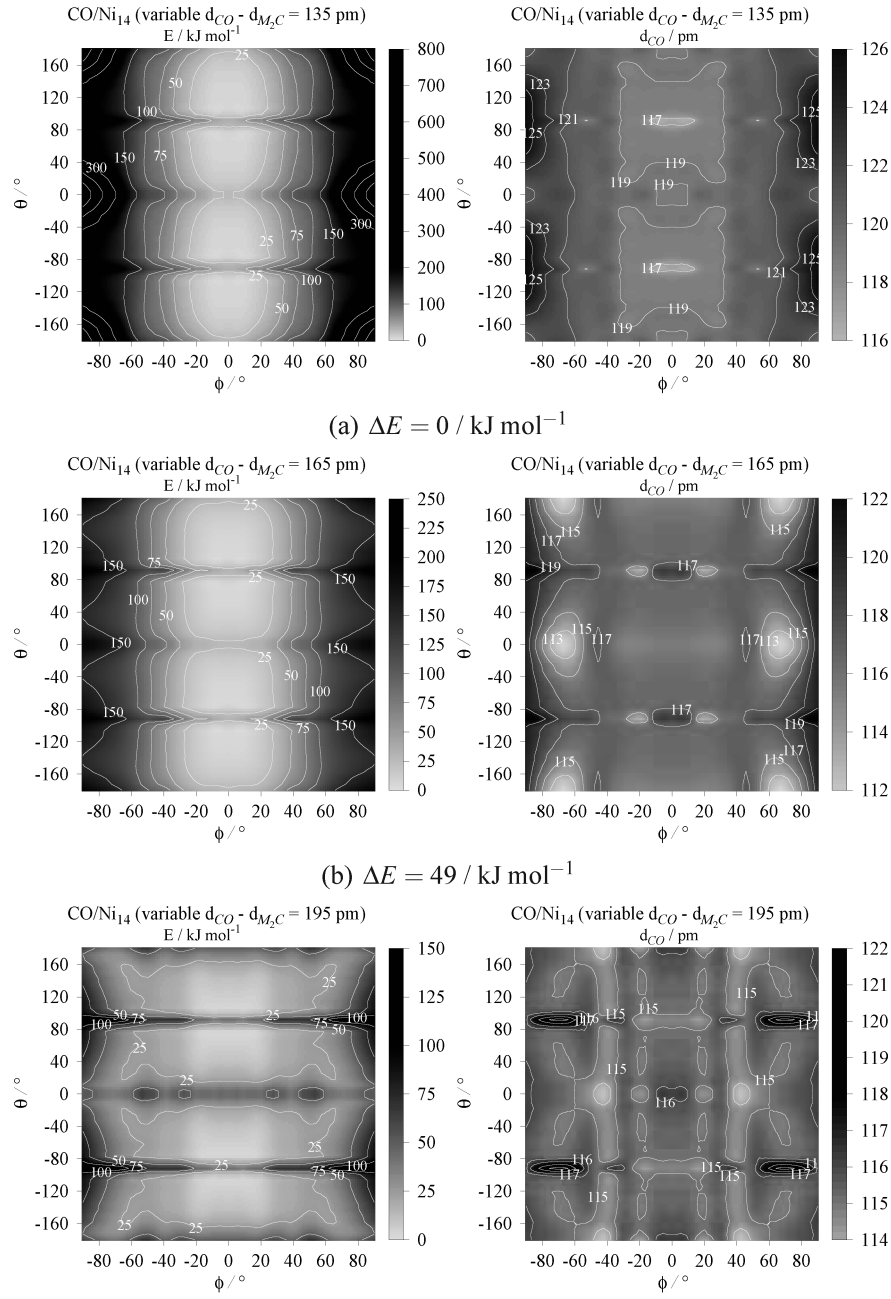

Figure 9. *PES*(θ,ϕ), *left column*, and *ESP*(θ,ϕ), *right column*, for the CO rotation (θ) and bending (ϕ) on the Ni_{14} fragment: d_{M_2C} is fixed (**a**) at the partially optimized equilibrium distance, 135 pm (*upper panels*), (**b**) at 165 pm (*midpanels*), and (**c**) at 195 pm (*lower panels*). *ESP*, for a given couple θ, ϕ, reports the d_{CO} value corresponding to the minimum energy point reported in the *PES*. The ΔE reported under each couple of panels is the difference between the energy minimum of each system and the lowest energy minimum found ($E_0 = -2483.3456$ au) for the three systems, assumed as reference.

fragments are similar to those of the smaller ones. Consequently, the findings achievable by the smaller Pd and Pt fragments, homogeneous to those of the larger ones, can be obtained at rather lower computational costs. The different behavior in the metals could occur because in the Ni system the M-M distance is about 10% shorter with respect to those of the Pd and Pt ones. As a consequence, the CO oxygen atom, for fixed d_{CO} values, can experience stronger interactions with the second Ni neighbors, during the surface rotations. Moreover, since the Ni_{14} fragment is ca. 50% in volume smaller if compared with the other metals, the third metal-atom plane is much closer to the CO molecule in the Ni system. So, the effects of the CO metal "bulk" interactions, either attractive or repulsive, are stronger, giving no consistent results between the two fragments. The equilibrium CO/M distances -- see Table 1 -- confirm this hypothesis, indicating the closer interaction between the CO molecule and the Ni cluster bulk. However, the behavior noticed in the smaller Ni fragment at high $|\phi|$ is somewhat confirmed in the larger system, with the existence of stability areas observed in broad regions around $\theta = 0°$ and $\theta = \pm 180°$.

In this area the energy is roughly constant for given ϕ values, analogous to what was observed with the smaller fragment. Noticeably, the *PES* of the Ni_{14} fragment at $\phi = 0°$ is at an energy about 20 kJ mol^{-1} higher than that shown in the neighboring region included in the range

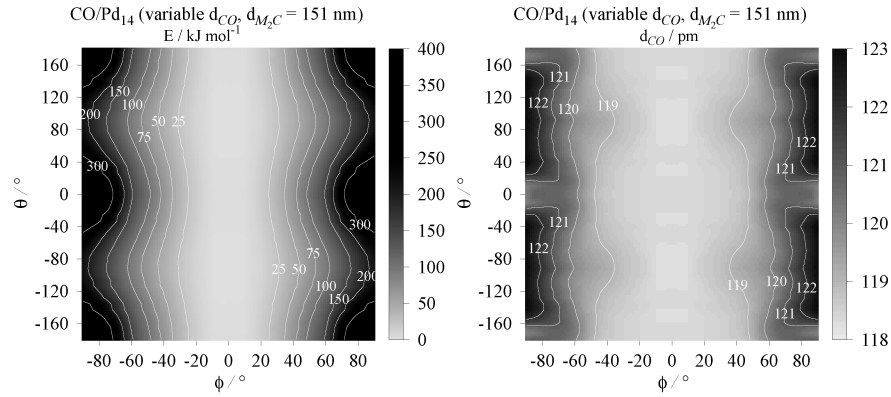

(a) $\Delta E = 0$ / kJ mol^{-1}

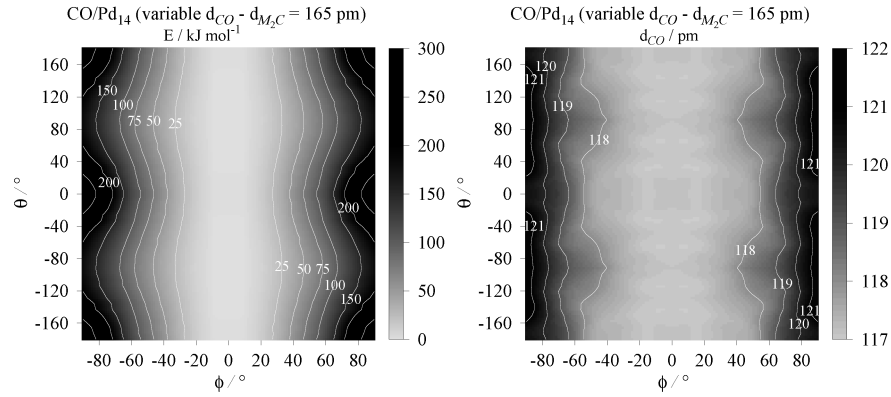

(b) $\Delta E = 26$ / kJ mol^{-1}

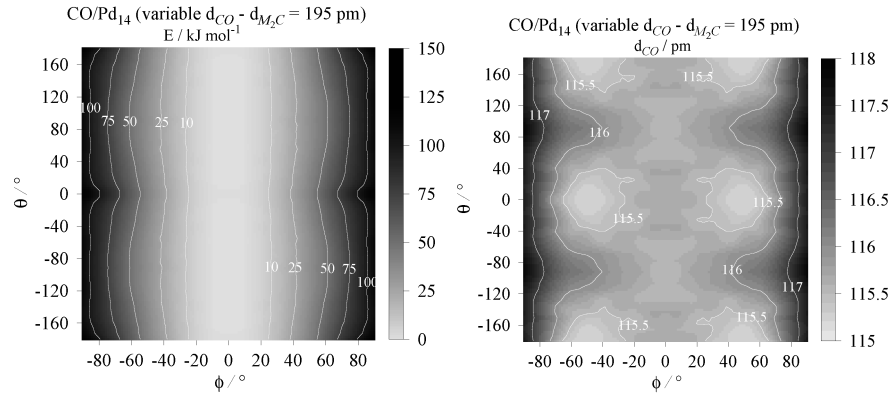

(c) $\Delta E = 102$ / kJ mol^{-1}

Figure 10. *PES*(θ,ϕ), *left column*, and *ESP*(θ,ϕ), *right column*, for the CO rotation (θ) and bending (ϕ) on the Pd_{14} fragment: d_{M_2C} is fixed (**a**) at the partially optimized equilibrium distance, 151 pm (*upper panels*), (**b**) at 165 pm (*midpanels*), and (**c**) at 195 pm (*lower panels*). *ESP*, for a given couple θ, ϕ, reports the d_{CO} value corresponding to the minimum energy point reported in the *PES*. The ΔE reported under each couple of panels is the difference between the energy minimum of each system and the lowest energy minimum found ($E_0 = -1887.8023$ au) for the three systems, assumed as reference.

$10° < |\phi| < 20°$. This would lead to the conclusion that the stablest CO configuration on the Ni surface could be slightly bent. Even so, this result does not agree with those obtained by the partial optimizations (both for the Ni_8 and Ni_{14} systems) or by the *PES* analysis with the Ni_8 fragment, where invariantly the energy minima has been found at $\phi = 0°$. This shows that a more realistic model is needed, in particular for the CO/Ni system, and this can be obtained by allowing changes of the C-O distance, as discussed in the next section where insights on the dependence of the CO properties from the d_{M_2C} values are contextually explored.

Adsorption of CO on M_{14} Fragments at Variable C-O and CO/M Distances. The models employed in this section have one additional degree of freedom with respect to those up to now considered. Moreover, for each system three different CO/M distances are carried out: i) the optimized distance reported in Table 1, ii) an average value comparable to that of the fixed C-O length systems (165 pm), and iii) a long-distance value (195 pm).

Provided, as explained in the Supporting Information, that every point in the θ, ϕ grid is associated with a minimum energy value $\{E(\theta,\phi)\}^m_\chi$ and with an equilibrium bond-length (at that energy) $\{d_{CO}(\theta,\phi)\}_\chi$, the energy and bond-length

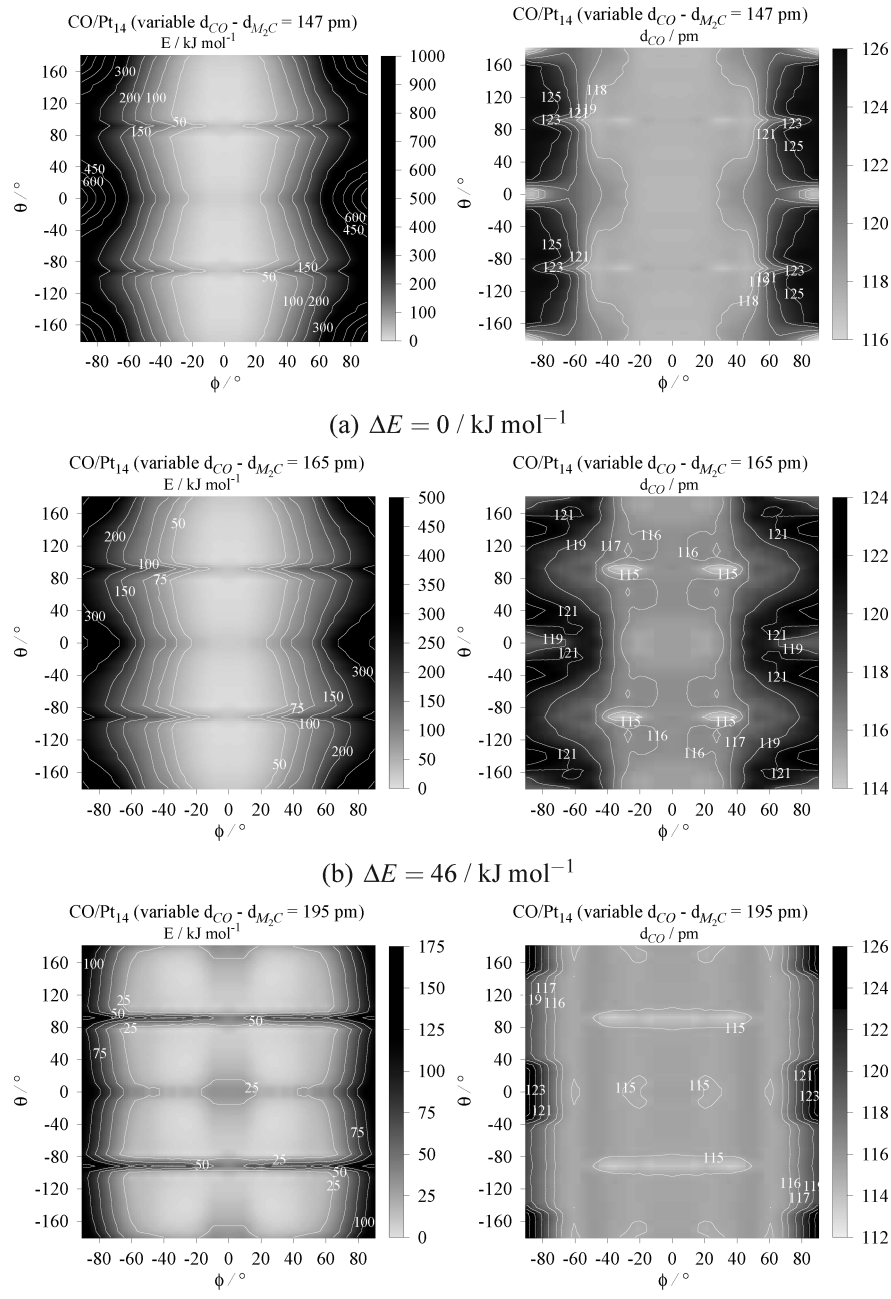

Figure 11. *PES*(θ,ϕ), *left column*, and *ESP*(θ,ϕ), *right column*, for the CO rotation (θ) and bending (ϕ) on the Pt_{14} fragment: d_{M_2C} is fixed (**a**) at the partially optimized equilibrium distance, 147 pm (*upper panels*), (**b**) at 165 pm (*midpanels*), and (**c**) at 195 pm (*lower panels*). *ESP*, for a given couple θ, ϕ, reports the d_{CO} value corresponding to the minimum energy point reported in the *PES*. The ΔE reported under each couple of panels is the difference between the energy minimum of each system and the lowest energy minimum found ($E_0 = -1781.4734$ au) for the three systems, assumed as reference.

points obtained are shown in a couple of the plots, *PES*(θ,ϕ) and *ESP*(θ,ϕ), reported in Figures 9−11. *PES*s show the energy minima obtained at given θ, ϕ couples, varying the d_{CO} parameter, whereas *ESP*s show the d_{CO} values at the same θ and ϕ, corresponding to the energy minima obtained along the d_{CO} variations. From the comparison of both *PES* and *ESP* plots it is possible to obtain interesting information on the configurational distribution, characterizing the different metal systems.

At first, it should be noticed that highly bent molecules are stabilized at larger distances from the *bcp* -- see Table 1 -- in all the metal systems. General observations also concern the CO bond-length, which coincides with the optimized one, at the equilibrium d_{M_2C} when $\phi = 0°$, and increases as $|\phi|$ does, irrespective of the d_{M_2C} value. This behavior, which presents few exceptions, can be explained since, increasing the $|\phi|$ value, the oxygen attractive interaction with the metal planes grows, causing the C-O bond-length rise. Moreover, all the *PES*s show their overall minima at $\phi = 0°$, irrespective of the considered d_{M_2C}, while for higher $|\phi|$ the energy behavior is not regular, scanning the three d_{M_2C} distances. By considering, at the same time, the energy increase at low, medium, and high $|\phi|$ and the minimum energy values of the three different *PES*s for a given metal, it is possible to confirm that the *PES* built at the d_{M_2C} equilibrium distance is always the most representa-

tive of the real system in the low $|\phi|$ region. However, the same equilibrium d_{M_2C} distance *PES* shows the largest energy gradient, as $|\phi|$ increases. Hence, the stablest system at intermediate and large $|\phi|$ are accounted for by the intermediate and large d_{M_2C} *PES*s, respectively.

These results show that the CO molecules move away from the surface when increasing their bending, confirming that i) the cartwheel and helicopter rotation energy barriers need d_{M_2C} changes to be taken into account and ii) the equilibrium distances calculated by optimizations, not considering bent molecules, are lacking in important information when studying average surface properties.

At the d_{M_2C} mid-distance (165 pm), the energy profiles of the Pd and Pt systems are similar to those already obtained at fixed C-O length. In particular, they are almost the same in the case of Pd, excluding for the energy increase at high $|\phi|$, which actually depends on the relative stabilization of the system occurring at lower $|\phi|$ values. Also in the case of Pt, the energy profiles are similar excluding for the presence in all the different d_{M_2C} systems of a narrow energetic instability region around $\theta = \pm 90°$, also stronger when the CO molecule is closer to the surface. This leads to the conclusion that the bending of the CO molecule is favored by θ angles slightly different from $\pm 90°$. Noticeably, the energy rise, increasing $|\phi|$, is larger for the Pt system as compared with the Pd one. Therefore, in the former the interaction ability of the CO molecules should be larger.

The analysis of the changes in the C-O bond-length with the angles displays other differences between the two metals. These can be mainly ascribed to the presence of the instability area around $\theta = \pm 90°$. For high $|\phi|$ values, the CO molecule indeed shows a detectable bond elongation on Pd (up to over 123 pm), corresponding to the lowest energy regions. This effect is common to all the d_{M_2C} systems but is stronger for the one with the CO molecule closer to the metal, while it is vanishing for the $d_{M_2C} = 195$ pm configuration. Conversely, the behavior of the CO bond-length sets two opposite effects on Pt. The first, dominant at the equilibrium d_{M_2C} value, shows analogously to the Pd systems a relationship between lower energy states and longer bonds, except for a wider range of bond-lengths allowed and for the narrow instability region at $\theta = \pm 90°$, coinciding with a shorter CO bond-length area. The second, characterizing the longest d_{M_2C} values, shows shorter bond-lengths corresponding to energy minima, around the energetic instability areas.

The Ni $PES(\theta,\phi)$ plots obtained by varying the d_{CO} distance -- see Figure 9 -- are different with respect to those obtained by fixing the same parameter. In particular, the absolute minimum was found at $\phi = 0°$, while energy maxima were determined at $\theta = 0°$ and $\pm 90°$ and relative minima at $\theta \approx \pm 45°$ and $\pm 135°$, the latter individuating typical bending regions for this metal. At the equilibrium distance (135 pm) the energy rise, increasing $|\phi|$, is very large, and consequently, as in the Pt system, a higher contribution of the configurations in which CO is more distant from the metal surface is expected for modeling the carbon monoxide bending on the metallic plane.

The C-O bond-length variations for the Ni_{14} fragment delineate a complex *ESP* behavior. A strong interaction of the CO molecule with the metal surface at the equilibrium distance could be deduced from the bond-length in the $\phi = 0°$ region. Moreover, as for the Pt systems, the C-O bond is elongated when the molecule is constrained in a bent position, indicating a strong interaction of the O atom, whereas at a variance with Pt, the C-O bond-length falls as d_{M_2C} increases.

Table 2. IR Stretching Parameters of Carbon Monoxide Adsorbed on Group 10 Metal Surfaces

CO/Ni_{14} system	$\tilde{\nu}_{CO}/cm^{-1}$	$\Delta\tilde{\nu}_{CO}/cm^{-1}$
W-ϕ[a]	1916	14
QC[b]	1879	—
Exp[c]	1900−1970	15
CO/Pd_{14} system	$\tilde{\nu}_{CO}/cm^{-1}$	$\Delta\tilde{\nu}_{CO}/cm^{-1}$
W-ϕ[a]	1953	8
QC[b]	1923	—
Exp[c]	1910−1964	15
CO/Pt_{14} system	$\tilde{\nu}_{CO}/cm^{-1}$	$\Delta\tilde{\nu}_{CO}/cm^{-1}$
W-ϕ[a]	1878	19
QC[b]	1860	—
Exp[c]	1845−1880	15

[a] Details on the evaluation protocol are given in the Supporting Information. On the whole, the $\tilde{\nu}_{CO}$ values are larger than those reported by Pacchioni et al.,[17] while they are in good agreement with those published by Curulla et al.[18] [b] The QC calculated stretching frequency value is corrected by considering the term 0.9613 as the empirical scaling factor.[33,34] [c] The average value of experimental findings derived from different works mostly referring to bridge adsorption on {100} metallic planes is reported in this row: Ni,[35] Pd,[36,37] Pt.[38]

It has to be recalled here that recent results by tdMC simulations[2,29] have i) pointed out the role of the CO steric hindrance in explaining "exotic phenomena"[31,32] present in CO reactions on Group 10 metal surfaces and ii) suggested that the steric hindrance should increase in the order Pd < Ni < Pt.[3] With respect to this, we observe both i) that the interaction energies involved in the CO/Pd and CO/Ni systems, occurring along the cartwheel and helicopter motions and varying the d_{CO} and d_{M_2C} values, are on the whole smaller than those of Pt and ii) that in the CO/Pd system the surface interaction energy maxima, which are present in the CO/Ni system, are also absent. These points would suggest that during the surface displacements the CO/Pd system is affected by weaker carbon monoxide metal-surface interactions than those of the CO/Ni system and the latter by weaker interactions than those of the CO/Pt one. Namely, the CO/M interaction energies on the Group 10 metal surfaces should rise in the same order found for the steric hindrance.

These aspects, which can be related to the electronic and relativistic properties[17] of the title CO/M systems, are discussed in more details at the end of the next section, taking into consideration the effects of the local interactions between the carbon monoxide and the metal-surface sites.

CO Stretching Band Recontruction. The $E(\theta,\phi)$ and $d_{CO}(\theta,\phi)$ values used to build the *PES*s and *ESP*s of the preceding section were further utilized to evaluate the frequency parameters of the C-O vibration of one carbon monoxide molecule adsorbed on {100} Ni, Pd, and Pt faces. In Table 2 the $\tilde{\nu}_{CO}$ and $\Delta\tilde{\nu}_{CO}$ values, obtained by the fits including the whole set of angles (W-ϕ) considered in the calculations, are shown for each metal along with the analogous QC and experimental (Exp) parameter values.

It is recalled that standard QC calculations of vibration frequencies are based on the analysis of coupled vibrational normal modes of the most stable molecular geometry and that a Gaussian inhomogeous broadening is added in a second step as an adjustable parameter.[33] At variance, the method presented here is aimed at facing "all" the allowed bridge surface-configurations, being for this accountable as a statistical method. As a consequence, the band position and broadening are evaluated by the population analysis of the considered molecular configurations. The $\tilde{\nu}_{CO}$ and $\Delta\tilde{\nu}_{CO}$ of each metal system were also calculated for selected groups of angles (i.e., configurations): $0° < |\phi| \leq 30°$, L-ϕ (low) set; $30° < |\phi| \leq 60°$, M-ϕ (mid) set; $60° < |\phi| \leq 90°$, H-ϕ (high) set.

The W-ϕ fit findings for the CO/Ni systems show a good agreement with the experimental results. By comparing the $\tilde{\nu}_{CO}$ and $\Delta\tilde{\nu}_{CO}$ values in the different ϕ ranges, it is worth noting that both the experimental and the W-ϕ fit values are larger than those found by using the L-ϕ and M-ϕ fits (1672 and 1838 cm^{-1}, respectively), indicating the relevance of the contribution of the bent states that are very significative in the H-ϕ range (2140 cm^{-1}). At variance with the Pd and Pt systems, the frequency characterizing the L-ϕ range is very different from the one obtained by the QC evaluation. We attribute such a characteristic to the strong interaction of the carbon monoxide with the bulk of the nickel fragment. The H-ϕ data set yields a very high frequency value, indicating a weak interaction of the bent CO molecule with the fragment surface. Finally, the frequencies obtained in different θ and ϕ ranges are not regular, accounting for the great variability of the CO behavior on the Ni cluster already reported for systems with variable surface coverage.[39]

The frequency calculations on the CO/Pd systems show a regular behavior. The frequency values fall in a narrower range, and the W-ϕ fit frequency value falls between those obtained by the L-ϕ and M-ϕ fits (1996 and 1946 cm^{-1}, respectively). Therefore, a relatively low contribution should arise from the H-ϕ bent states (frequency at 1786 cm^{-1}). The frequency behavior determined in the three partial ϕ ranges shows an opposite trend with respect to that of Ni, decreasing $\tilde{\nu}_{CO}$ with increasing $|\phi|$. Moreover, the frequency values obtained in the L-ϕ range are consistent with a weaker interaction of the CO molecule with the metal surface, in the case of Pd respecting that of Ni and Pt fragments -- see below. This could be rationalized considering that the equilibrium distance of the CO molecule with the Pd *bcp* is the largest among the three metals. Thus, the significant interaction between the CO molecule and the cluster in this system probably extends also at a longer distance from the surface than those considered in the present study.

In the CO/Pt systems as in the Ni ones, the frequency increases as the molecular bending does. In fact, in the L-ϕ and M-ϕ intervals the frequency values (1865 and 1885 cm^{-1}, respectively) are similar to the experimental ones, while the H-ϕ frequency is higher (2064 cm^{-1}), indicating a reduced interaction with the metal fragment for large $|\phi|$ values. These results confirm that the Pt system is characterized by characteristics common both to those of the Ni and Pd ones.

Interestingly, the calculated W-ϕ frequencies in agreement with the experimental results increase in the following order: Pd > Ni > Pt. The latter trend is consistent with the opposite one found for the CO/M surface interaction energies. This occurrence is not surprising, since $\tilde{\nu}_{CO}$ decreases, weakening and lengthening the C-O bond,[40] as the CO/M surface interaction energies increase.

The average band-broadening obtained for the experimental IR band is ca. 15 cm^{-1}, irrespective of the considered metal. This value is well reproduced by the W-ϕ fit performed on the Ni and Pt fragments, whereas on the Pd one the calculated band-broadening is slightly smaller. In fact, the analysis of the values in the different ϕ ranges shows that the main contribution to the broadening originates from the H-ϕ ranges, where the molecule-surface distances increase and the corresponding interactions decrease. The lack of a sufficiently populated long-distance configuration set, as above hypothesized for the Pd system, could hence reduce the band broadening value. However, we have to be aware that the comparison of experimental and calculated IR results has to embody not only the frequency contributions given by the different surface configurations but also the band changes originated by molecular lateral interactions that are not considered here.

The IR frequencies characterizing the stretching of the CO molecules on the different metals confirm a variable ability of mutual interaction. As already recalled, higher CO stretching frequencies indicate weaker surface interaction strengths hence larger local mobility and adaptability. This means on the whole that the adsorbed CO molecules exert and feel less steric hindrance, increasing the C-O stretching frequencies. Then, by the present findings and in accord with recent MC results[3] the steric hindrance of the carbon monoxide should increase on Pd, Ni, and Pt, in the order. This agrees with the *PES* results obtained at variable d_{M_2C} values.

A simple molecular-level explanation of the behavior of the CO/M interaction energetics, the C-O stretching frequency, and the CO/M steric hindrance on Group 10 metal surfaces is clearly not straightforward. However, a phenomenological link can be found with the $\Delta_{CO/M} = d_{M_2C} - r_M$ difference, with r_M being the radius of a given Group 10 atom. The $\Delta_{CO/M}$ parameter, which for Pd, Ni, and Pt is 13.(5), 10.(5), and 8.(5) pm, gives an evaluation of the distance of the carbon atom from the metal electronic surface,[14] whose properties are related to the surface energy of the same metals.[41] The $\Delta_{CO/M}$ values actually suggest that the CO molecule feels larger electronic surface effects by Pt > Ni > Pd fragments and as a result experience in the same order larger surface energy, like experimentally and theoretically predicted.[41] Coherently, in the same order the carbon monoxide metal-surface interaction energy increases, as does the CO/M steric hindrance, while the C-O stretching frequency decreases.

CONCLUSIONS

From a methodological point of view, it is possible to conclude that the smaller crystallite fragment can model qualitative characteristics of the energetic profile, which occur along the CO adsorption on Pd and Pt. For the Ni systems, the behavior of the M_8 and M_{14} fragments, due to the smaller sizes of the metal atoms, is slightly different and suggests the use of the larger models, also taking into consideration the variations of the C-O and the CO/M distances.

In the larger models, the behavior of the three metals could be rationalized on the basis of the different interaction

energies. The Ni systems suggest a stabilization both of the surface-configurations in which the O atom is pointing toward a metal atom and of the slanted configurations with respect to the perpendicular ones, increasing the d_{M_2C} distances. The relative stabilization of the bent molecules at large d_{M_2C} distances can be also hypothesized, although to a lesser extent, for the Pt systems. Conversely, the Pd systems have a very regular behavior, showing a typical bond elongation occurring when the O atom is pointing between two metal atoms. The Pt systems, whose *PES*s are similar to those of Pd except for an instability region at $\theta = \pm 90°$, show characteristic shorter bonds corresponding to energetic minima at larger d_{M_2C} values.

The IR frequencies and band-broadenings of the adsorbed CO models were determined by sampling the set of the considered surface-configurations achievable in the different systems, at a variance with the customary QC approaches that allow one to determine just the frequency values, considering the molecular geometry at the energy minimum. Good agreement with the experimental frequency results was obtained for all the metals. Reliable band-broadenings were obtained for the CO/Ni and CO/Pt systems, while the CO/Pd system yielded a lower band-broadening value, related to the consideration of a reduced configurational sampling space characterizing the latter system.

The interaction energetics, the steric hindrance, and the stretching properties of the adsorbed carbon monoxide molecule can be collectively associated with the electronic characteristics of the considered metallic systems and phenomenologically can be referred to the relative distance of the CO molecule from the electronic surfaces of the same metallic fragments.

ACKNOWLEDGMENT

This work was supported by the NANOCAT Project -- funded in the frame of the 6th Framework Programme of the European Community, Contract No. NMP3-CT-2005-506621, by the Italian Ministero dell'Università e della Ricerca and by the University of Palermo. Prof. Gianfranco La Manna is thanked for critical discussions on the subject and for careful reading of the manuscript.

Supporting Information Available: Details on the evaluation protocol. This material is available free of charge via the Internet at http://pubs.acs.org.

REFERENCES AND NOTES

(1) (a) Boudart, M.; Djega-Mariadassou, G. *Kinetics of Heterogeneous Catalytic Reactions*; Princeton U. Press: Princeton NJ, 1984; pp 38−76. (b) Dumesic, J. A.; Rudd, D. F.; Aparicio, L. M.; Rekoske, J. E.; Trevino, A. A. *The Microkinetics of Heterogeneous Catalysis*; ACS Professional Reference Book: Washington, DC, 1993; pp 1−72. (c) van Santen, R. A.; Neurock, M. *Molecular Heterogeneous Catalysis*; Wiley-VCH: Weinheim, 2006; pp 19−82.

(2) (a) Duca, D.; Botár, L.; Vidóczy, T. Monte Carlo simulation of ethylene hydrogenation on Pt catalysts. *J. Catal.* **1996**, *162*, 260–267. (b) Duca, D.; Baranyai, P.; Vidóczy, T. Monte-Carlo model for the hydrogenation of alkenes on metal catalyst. *J. Comput. Chem.* **1998**, *19*, 396–403. (c) Duca, D.; Barone, G. Varga, Zs. Hydrogenation of acetylene-ethylene mixtures on Pd catalysts: computational study on the surface mechanism and on the influence of the carbonaceous deposits. *Catal. Lett.* **2001**, *72*, 17–23. (d) Barone, G.; Duca, D. Hydrogenation of 2,4-dinitro-toluene on Pd/C catalysts: computational study on the influence of the molecular adsorption modes and of steric hindrance and metal dispersion on the reaction mechanism. *J. Catal.* **2002**, *211*, 296–307.

(3) Duca, D.; Barone, G.; Giuffrida, S. Varga, Zs. IDEA: Interface dynamics and energetics algorithm. *J. Comput. Chem.* **2007**, *28*, 2483–2499.

(4) (a) Kopf, A.; Baschnagel, J.; Wittmer, J.; Binder, K. On the adsorption process in polymer brushes: a Monte Carlo study. *Macromolecules* **1996**, *29*, 1433–1441. (b) Borodzínski, A. Hydrogenation of acetylene-ethylene mixtures on a commercial palladium catalyst. *Catal. Lett.* **1999**, *63*, 35–42. (c) Couvreur, P.; Gref, R.; Andrieux, K.; Malvy, C. Nanotechnologies for drug delivery: application to cancer and autoimmune diseases. *Prog. Solid State Chem.* **2006**, *34*, 231–235. (d) Delbecq, F.; Zaera, F. Origin of the selectivity for trans-to-cis isomerization in 2-butene on Pt(111) single crystal surfaces. *J. Am. Chem. Soc.* **2008**, *130*, 14924–14925.

(5) (a) Behm, R. J.; Christmann, K.; Ertl, G.; van Hove, M. A. Adsorption of CO on Pd(100). *J. Chem. Phys.* **1980**, *73*, 2984–2995. (b) Ferrari, A. M.; Neyman, K. M.; Belling, T.; Mayer, M.; Rötsch, N. Small platinum clusters in zeolites: a Density-functional study of CO adsorption on electronically modified models. *J. Phys. Chem. B* **1999**, *103*, 216–226.

(6) Doll, K. CO adsorption on the Pt(111) surface: a comparison of a gradient corrected functional and a hybrid functional. *Surf. Sci.* **2004**, *573*, 464–473.

(7) Abild-Pedersen, F.; Andersson, M. P. CO adsorption energies on metals with correction for high coordination adsorption sites -- a density-functional study. *Surf. Sci.* **2007**, *601*, 1747–1753.

(8) Perrier, A.; Bonnet, L.; Rayez, J.-C. Dynamical study of H_2 and D_2 desorbing from a Cu(111) surface. *J. Phys. Chem. A* **2006**, *110*, 1608–1617.

(9) (a) Yeo, Y. Y.; Wartaby, C. E.; King, D. A. Calorimetric measurement of the energy difference between two solid surface phases. *Science* **1995**, *268*, 1731–1732. (b) Brown, W. A.; Kose, R.; King, D. A. Femtomole adsorption calorimetry on single-crystal surfaces. *Chem. Rev.* **1998**, *98*, 797–832. (c) Kim, M.; Bertram, M.; Pollmann, M.; von Oertzen, A.; Mikhailov, A. S.; Rotermund, H. H.; Ertl, G. Controlling chemical turbulence by global delayed feedback: pattern formation in catalytic CO oxidation on Pt(110). *Science* **2001**, *292*, 1357–1360. (d) Li, W.; Gracia, F. J.; Wolf, E. E. Selective combinatorial catalysis; challenges and opportunities: the preferential oxidation of carbon monoxide. *Catal. Today* **2003**, *81*, 437–447. (e) Snytnikov, P. V.; Sobyanin, V. A.; Belyaev, V. D.; Tsyrulnikov, P. G.; Shitova, N. B.; Shlyapin, D. A. Selective oxidation of carbon monoxide in excess hydrogen over Pt-, Ru- and Pd-supported catalysts. *Appl. Catal., A* **2003**, *239*, 149–156. (f) Irurzun, I. M.; Hoyle, R. B.; Proctor, M. R. E.; King, D. A. Modelling pattern formation in CO + O_2 on Pt{100}. *Chem. Phys. Lett.* **2003**, *377*, 269–278.

(10) (a) Bianchini, C.; Meli, A. Alternating copolymerization of carbon monoxide and olefins by single-site metal catalysis. *Coord. Chem. Rev.* **2002**, *225*, 35–66. (b) Chen, P.; Westerberg, S.; Kung, K. Y.; Zhu, J.; Grunes, J.; Somorjai, G. A. CO poisoning of catalytic ethylene hydrogenation on the Pt(111) surface studied by surface sum frequency generation. *Appl. Catal., A* **2002**, *229*, 147–154. (c) Grunes, J.; Zhu, J.; Yang, M.; Somorjai, G. A. CO poisoning of ethylene hydrogenation over Pt catalysts: a comparison of Pt(111) single crystal and Pt nanoparticle activities. *Catal. Lett.* **2003**, *86*, 157–161.

(11) (a) Masel, R. I. *Principles of Adsorption and Reaction on Solid Surfaces --Wiley Series in Chemical Engineering*; Wiley: New York, 1996; pp 563−564. (b) Nibbelke, R.; Nievergeld, A. J. L.; Hoebink, J. H. B. J.; Marin, G. B. Development of a transient kinetic model for the CO oxidation by O_2 over a Pt/Rh/CeO_2/γ-Al_2O_3 three-way catalyst. *Appl. Catal., B* **1998**, *19*, 245–259.

(12) Jager, B. Developments in Fischer−Tropsch Technology. In *Natural Gas Conversion*; Parmaliana, A., Sanfilippo, D., Frusteri, F., Vaccari, A., Arena, F., Eds.; Elsevier: New York, 1998; Vol. 5, pp 25−34.

(13) (a) Paukshtis, E. A. Infrared spectroscopy to study the mechanism of catalytic reaction on molecular scale from diffusion to limiting stage kinetics. *J. Mol. Catal. A: Chem.* **2000**, *158*, 37–44. (b) Tsyganenko, A. A.; Storozhev, P. Yu.; Areán, C. O. IR-spectroscopic study of the binding isomerism of adsorbed molecules. *Kinet. Catal.* **2004**, *45*, 530.

(14) Ashcroft, N.; Mermin, N. *Solid State Physics*; HRW International Editions: Philadelphia, 1976; pp 86−94.

(15) (a) Andersson, S. Vibrational excitations and structure of CO adsorbed on Ni(100). *Solid State Commun.* **1977**, *21*, 75–81. (b) Lauterbach, J.; Wittmann, M.; Küppers, J. Adsorption of CO at Ni(100) surfaces: a FTIRAS-TDS study. *Surf. Sci.* **1992**, *279*, 287–296.

(16) Stuckless, J. T.; Al-Sarraf, N.; Wartnaby, C.; King, D. A. Calorimetric heats of adsorption for CO on nickel single crystal surfaces. *J. Chem. Phys.* **1993**, *99*, 2202–2212.

(17) Pacchioni, G.; Chung, S.-C.; Krüger, S.; Rösch, N. Is CO chemisorbed on Pt anomalous compared with Ni and Pd? An example of surface chemistry dominated by relativistic effects. *Surf. Sci.* **1997**, *392*, 173–184.

(18) Curulla, D.; Clotet, A.; Ricart, J. M. Ab-initio cluster model study of the chemisorption of CO on low-index platinum surfaces. *J. Phys. Chem. B* **1999**, *103*, 5246–5255.

(19) Frisch, M. J.; Trucks, G. W.; Schlegel, H. B.; Scuseria, G. E.; Robb, M. A.; Cheeseman, J. R.; Montgomery, J. A., Jr.; Vreven, T.; Kudin, K. N.; Burant, J. C.; Millam, J. M.; Iyengar, S. S.; Tomasi, J.; Barone, V.; Mennucci, B.; Cossi, M.; Scalmani, G.; Rega, N.; Petersson, G. A.; Nakatsuji, H.; Hada, M.; Ehara, M.; Toyota, K.; Fukuda, R.; Hasegawa, J.; Ishida, M.; Nakajima, T.; Honda, Y.; Kitao, O.; Nakai, H.; Klene, M.; Li, X.; Knox, J. E.; Hratchian, H. P.; Cross, J. B.; Bakken, V.; Adamo, C.; Jaramillo, J.; Gomperts, R.; Stratmann, R. E.; Yazyev, O.; Austin, A. J.; Cammi, R.; Pomelli, C.; Ochterski, J. W.; Ayala, P. Y.; Morokuma, K.; Voth, G. A.; Salvador, P.; Dannenberg, J. J.; Zakrzewski, V. G.; Dapprich, S.; Daniels, A. D.; Strain, M. C.; Farkas, O.; Malick, D. K.; Rabuck, A. D.; Raghavachari, K.; Foresman, J. B.; Ortiz, J. V.; Cui, Q.; Baboul, A. G.; Clifford, S.; Cioslowski, J.; Stefanov, B. B.; Liu, G.; Liashenko, A.; Piskorz, P.; Komáromi, I.; Martin, R. L.; Fox, D. J.; Keith, T.; Al-Laham, M. A.; Peng, C. Y.; Nanayakkara, A.; Challacombe, M.; Gill, P. M. W.; Johnson, B.; Chen, W.; Wong, M. W.; Gonzalez, C.; Pople, J. A. *Gaussian 03, Revision D.02*; Gaussian, Inc.: Wallingford, CT, 2005.

(20) (a) Becke, A. D. Density-functional thermochemistry. III. The role of exact exchange. *J. Chem. Phys.* **1993**, *98*, 5648–5652. (b) Stephens, P. J.; Devlin, J. F.; Chabalowsky, C. F.; Frisch, M. J. Ab-initio calculation of vibrational absorption and circular dichroism spectra using density-functional force fields. *J. Phys. Chem.* **1994**, *98*, 11623–11627.

(21) Hay, P. J.; Wadt, W. R. Ab-initio effective core potentials for molecular calculations. Potentials for the transition metal atoms Sc to Hg. *J. Chem. Phys.* **1985**, *82*, 270–283.

(22) Wu, Z. J.; Shi, J. S.; Zhang, S. Y.; Zhang, H. J. Density-functional study of lanthanum, ytterbium, and lutetium dimers. *Phys. Rev. A* **2004**, *69*, 064502.1064502.4.

(23) Levine, N. I. *Quantum Chemistry*, 5th ed.; Prentice Hall: Upper Saddle River, NJ, 1999; pp 587−589.

(24) Cramer, C. J. *Essentials of Computational Chemistry -- Theories and Models*, 2nd ed.; John Wiley & Sons, Ltd.: Chichester, 2004; pp 86−89, 273.

(25) Boys, S. F.; Bernardi, F. The calculation of small molecular interactions by the differences of separate total energies. Some procedures with reduced errors. *Mol. Phys.* **1970**, *19*, 553–566.

(26) Yeo, Y. Y.; Vattuone, L.; King, D. A. Calorimetric investigation of NO and CO adsorption on Pd{100} and the influence of preadsorbed carbon. *J. Chem. Phys.* **1997**, *106*, 1990–1996.

(27) Yeo, Y. Y.; Vattuone, L.; King, D. A. Energetics and kinetics of CO and NO adsorption on Pt{100}: Restructuring and lateral interactions. *J. Chem. Phys.* **1996**, *104*, 3810–3821.

(28) All *PES*s reported in the following have been obtained by a differential approach. In this, the points of each plot are referred, by a difference, to the minimum value present in the same plot, which consequently is taken as 0. For the sake of simplicity, from now on, the term *PES* is considered a synonym of differential *PES*.

(29) (a) Duca, D.; La Manna, G.; Russo, M. R. Computational studies on surface reaction mechanisms: ethylene hydrogenation on platinum catalysts. *Phys. Chem. Chem. Phys.* **1999**, *1*, 1375–1382. (b) Duca, D.; La Manna, G.; Varga, Zs.; Vidóczy, T. Hydrogenation of acetylene-ethylene mixtures on Pd catalysts: study of the surface mechanism by computational approaches. Metal dispersion and catalytic activity. *Theor. Chem. Acc.* **2000**, *104*, 302–311.

(30) CO first neighbors are the metal-atoms on which the CO molecule is directly adsorbed, while the CO second neighbors are the metal-atoms vicinal to the first neighbors.

(31) Wintterlin, J.; Schuster, R.; Ertl, G. Existence of a "Hot" Atom mechanism for the dissociation of O_2 on Pt(111). *Phys. Rev. Lett.* **1996**, *77*, 123–126.

(32) (a) Yamada, T.; Onishi, T.; Tamaru, K. Adsorption-desorption kinetics of carbon monoxide on palladium polycrystalline surfaces. *Surf. Sci.* **1983**, *133*, 533–546. (b) Boudart, M. Adsorption assisted desorption in catalytic cycles. *J. Mol. Catal. A: Chem.* **1999**, *141*, 1–7.

(33) Foresman, J. B.; Frisch, Æ. *Exploring Chemistry with Electronic Structure Methods*, 2nd ed.; Gaussian Inc.: Pittsburgh, PA, 1996; pp 61−90.

(34) Scott, A. P.; Radom, L. Harmonic vibrational frequencies: an evaluation of Hartree-Fock, Möller-Plesset, quadratic configuration interaction, density-functional theory, and semiempirical scale factors. *J. Phys. Chem.* **1996**, *100*, 16502–16513.

(35) (a) Compuzano, J. C.; Greenler, R. G. The adsorption sites of CO on Ni(111) as determined by infrared reflection-absorption spectroscopy. *Surf. Sci.* **1979**, *83*, 301–312. (b) Coulter, K.; Xu, X.; Goodman, D. W. Structural and catalytic properties of model supported nickel catalysts. *J. Phys. Chem.* **1994**, *98*, 1245–1249. (c) Smirnov, K. S.; Raseev, G. Coverage dependent IR frequency shift of CO molecules adsorbed on Ni(111) surface. *Surf. Sci.* **1997**, *384*, L875–L879. (d) Bandara, A.; Katano, S.; Kubota, J.; Onda, K.; Wada, A.; Domen, K.; Hirose, C. The effect of CO-adsorption of on-top CO on the sum-frequency generation signal of bridge CO on the Ni(111) surface. *Chem. Phys. Lett.* **1998**, *290*, 261–267.

(36) (a) Loffreda, D.; Simon, D.; Sautet, P. Dependence of stretching frequency on surface coverage and adsorbate-adsorbate interactions: a density-functional theory approach of CO on Pd (111). *Surf. Sci.* **1999**, *425*, 68–80. (b) Ozensoy, E.; Meier, D. C.; Goodman, D. Polarization modulation infrared reflection-absorption spectroscopy at elevated pressures: CO adsorption on Pd(111) at atmospheric pressures. *J. Phys. Chem. B* **2002**, *106*, 9367–9371.

(37) Morkel, M.; Unterhalt, H.; Klüner, T.; Rupprechter, G.; Freund, H.-J. Interpreting intensities in vibrational sum frequency generation (SFG) spectroscopy: CO adsorption on Pd surfaces. *Surf. Sci.* **2005**, *586*, 146–156.

(38) (a) Robbins, J. L.; Marucchi-Soos, E. Observation of combination modes in transmission IR spectra of carbon monoxide on supported platinum. *J. Phys. Chem.* **1987**, *91*, 2026–2028. (b) Hong, S.; Richardson, H. H. Infrared reflection-absorption spectroscopy of adsorbates on a platinum (100) surface during carbon monoxide oxidation. *J. Phys. Chem.* **1993**, *97*, 1258–1261. (c) Somorjai, G. A.; Su, X.; McCrea, K. R.; Rider, K. B. Molecular surface studies of adsorption and catalytic reaction on crystal (Pt, Rh) surfaces under high pressure conditions (atmospheres) using sum frequency generation (SFG) -- surface vibrational spectroscopy and scanning tunneling microscopy (STM). *Top. Catal.* **1999**, *8*, 23–34.

(39) Eichler, A. CO adsorption on Ni(111) -- a density-functional theory study. *Surf. Sci.* **2003**, *526*, 332–340.

(40) Harris, D. C.; Bertolucci, M. D. *Symmetry and Spectroscopy*; Oxford University Press: New York, 1978; pp 62−117.

(41) (a) Tyson, W. R.; Miller, W. A. Surface free energies of solid metals: estimation from liquid surface tension measurements. *Surf. Sci.* **1977**, *62*, 267–276. (b) Foiles, S. M.; Baskes, M. I.; Daw, M. S. Embedded-atom-method functions for the fcc metals Cu, Ag, Au, Ni, Pd, Pt, and their alloys. *Phys. Rev. B* **1986**, *33*, 7983–7991.

CI800469M